AD_____

CONTRACT NUMBER DAMD17-95-C-5080

TITLE: MR Microscope for Use in Histology

PRINCIPAL INVESTIGATOR: R.S. Withers, Ph.D.
G. A. Johnson, Ph.D.; M. Yap, M.S.; S.E. Hurlston, B.S.; W. W. Brey, Ph.D.

CONTRACTING ORGANIZATION: Conductus, Inc.
Sunnyvale, California 94086

REPORT DATE: September 1996

TYPE OF REPORT: Final

PREPARED FOR: Commander
U.S. Army Medical Research and Materiel Command
Fort Detrick, Frederick, Maryland 21702-5012

DISTRIBUTION STATEMENT: Approved for public release;
distribution unlimited

The views, opinions and/or findings contained in this report are those of the author(s) and should not be construed as an official Department of the Army position, policy or decision unless so designated by other documentation.

DTIC QUALITY INSPECTED 2

19970224 054

REPORT DOCUMENTATION PAGE

Form Approved
OMB No. 0704-0188

Public reporting burden for this collection of information is estimated to average 1 hour per response, including the time for reviewing instructions, searching existing data sources, gathering and maintaining the data needed, and completing and reviewing the collection of information. Send comments regarding this burden estimate or any other aspect of this collection of information, including suggestions for reducing this burden, to Washington Headquarters Services, Directorate for Information Operations and Reports, 1215 Jefferson Davis Highway, Suite 1204, Arlington, VA 22202-4302, and to the Office of Management and Budget, Paperwork Reduction Project (0704-0188), Washington, DC 20503.

1. AGENCY USE ONLY *(Leave blank)*

2. REPORT DATE
September 1996

3. REPORT TYPE AND DATES COVERED
Final (21 Aug 95 - 20 Aug 96)

4. TITLE AND SUBTITLE
MR Microscope for Use in Histology

5. FUNDING NUMBERS
DAMD17-95-C-5080

6. AUTHOR(S)
R.S. Withers, Ph.D., W.W. Brey, Ph.D., G.A. Johnson, Ph.D.
M. Yap, M.S., S.E. Hurlston, B.S.

7. PERFORMING ORGANIZATION NAME(S) AND ADDRESS(ES)
Conductus, Inc.
Sunnyvale, California 94086

8. PERFORMING ORGANIZATION REPORT NUMBER

9. SPONSORING/MONITORING AGENCY NAME(S) AND ADDRESS(ES)
Commander
U.S. Army Medical Research and Materiel Command
Fort Detrick, Frederick, MD 21702-5012

10. SPONSORING/MONITORING AGENCY REPORT NUMBER

11. SUPPLEMENTARY NOTES

12a. DISTRIBUTION / AVAILABILITY STATEMENT
Approved for public release; distribution unlimited

12b. DISTRIBUTION CODE

13. ABSTRACT *(Maximum 200*

The long-term goal of this project is to develop a magnetic resonance microscope (MRM) suitable for providing sufficiently rapid assessment of tissue pathology to guide surgery. In this first phase of the project, a feasibility study has been performed. Sensitivity is the key technical issue to developing a practical MRM for clinical applications, so two issues that are crucial to sensitivity have been evaluated: the strength of the polarizing field and the design of the RF coil. The optimal strength of the polarizing field was evaluated based on the contrast to noise ratio (CNR) of a T1 weighted image. For a wide range of relaxation parameters there was a pronounced peak in the CNR at fairly low field. The choice of such a magnetic field would dramatically reduce the cost and size of the final instrument. The performance of HTS and copper RF coils was compared in a 2.0 T MRI system. Even under conditions that were far from ideal, a factor of two improvement in sensitivity was obtained with HTS coils. The results point to a new strategy for providing high contrast and resolution in a relatively inexpensive, compact instrument.

14. SUBJECT TERMS
microscope, NMR, MRI, superconductor

15. NUMBER OF PAGES
28

16. PRICE CODE

17. SECURITY CLASSIFICATION OF REPORT	18. SECURITY CLASSIFICATION OF THIS PAGE	19. SECURITY CLASSIFICATION OF ABSTRACT	20. LIMITATION OF ABSTRACT
Unclassified	Unclassified	Unclassified	Unlimited

FOREWORD

Opinions, interpretations, conclusions and recommendations are those of the author and are not necessarily endorsed by the U.S. Army.

( ) Where copyrighted material is quoted, permission has been obtained to use such material.

( ) Where material from documents designated for limited distribution is quoted, permission has been obtained to use the material.

( ) Citations of commercial organizations and trade names in this report do not constitute an official Department of the Army endorsement or approval of the products or services of these organizations.

( ) In conducting research using animals, the investigator(s) adhered to the "Guide for the Care and Use of Laboratory Animals," prepared by the Committee on Care and Use of Laboratory Animals of the Institute of Laboratory Animal Resources, National Research Council (NIH Publication No. 86-23, Revised 1985).

( ) For the protection of human subjects, the investigator(s) have adhered to policies of applicable Federal Law 32 CFR 219 and 45 CFR 46.

( ) In conducting research utilizing recombinant DNA technology,the investigator(s) adhered to current guidelines promulgated by the National Institutes of Health.

Principal Investigator's Signature Date 2 Dec. 96

INTRODUCTION **3**

ANTICIPATED BENEFITS / POTENTIAL COMMERCIAL APPLICATIONS 3

BACKGROUND OF PREVIOUS WORK 3

I. History: *3*

II. Resolution Limits in MR imaging: *4*

III. Contrast: *5*

IV. Discussion: *6*

OTHER PROGRAMS 7

HTS COIL DEVELOPMENT **8**

COOLING APPARATUS 8

COIL DESIGNS 8

COIL FABRICATION AND TESTING 11

SURFACE COIL IMAGING WITH HTS COILS 15

THE FIELD DEPENDENCE OF CONTRAST TO NOISE IN MAGNETIC RESONANCE MICROSCOPY **20**

FIELD DEPENDENCE OF SIGNAL TO NOISE 20

FIELD DEPENDENCE OF T_1 20

CONTRAST TO NOISE 21

CONCLUSIONS **23**

TECHNOLOGY DEVELOPMENT 23

POTENTIAL APPLICATIONS 23

BIBLIOGRAPHY **24**

REFERENCES **24**

Introduction

The long-term goal of this project is to develop a magnetic resonance microscope (MRM) suitable for providing sufficiently rapid assessment of tissue pathology to guide surgery. The specific goal of this phase of the project was to determine an appropriate field strength for the operation of the clinical NMR microscope, and to develop the required coil technology. This includes demonstrating the SNR gain obtainable with an HTS coil. Conventional optical staining, although very effective in diagnosis, is an overnight procedure and for this reason is of limited value in an operating-room (OR) environment. The proposed clinical MRM uses thin-film transmit/receive coils of YBCO ($Y_1Ba_2Cu_3O_7$), a high-temperature superconductor (HTS). The YBCO coil will provide an improvement in signal-to-noise ratio (SNR) of a factor of up to ten 10 compared to conventional copper coils. This SNR gain can be used to obtain greater spatial resolution or, alternatively, to reduce the time needed to acquire an image by a factor of up to 100. Consequently, pathology assessments that at present take 24-36 hours can be performed in less than 30 minutes, making MRM a clinically viable tool.

The program has contained two distinct elements: (1) development of an MRM at 2.0 T for the study of larger specimens at lower resolution; and (2) expansion of the knowledge base of NMR contrast mechanisms and their clinical value in histology. A probe subsystem based on HTS technology has been developed to perform small-animal and specimen imaging experiments at 2.0 T. Also, the dependence of contrast to noise ratio on magnetic field strength has been modeled as a function of magnetic field.

Anticipated benefits / potential commercial applications

The goal of this effort is to develop MR microscopes for use in a clinical environment. This instrument offers contrast unobtainable by standard optical staining techniques, true three-dimensional imaging, and rapid yield of data for guiding surgery. The commercial market is estimated at over $10,000,000 per year.

Background of Previous Work

I. History:

Nuclear magnetic resonance (NMR) has been one of the essential tools for chemists for more than forty years. In 1973, Paul Lauterbur described an experiment that formed the basis of one of the most exciting revolutions in modern medicine[1]. In that experiment, Lauterbur noted that the position of multiple proton sources could be differentiated by the application of a magnetic field gradient during the acquisition of a free induction decay. From the onset, it was clear that this phenomenon could be extended into the microscopic domain. Soon after, Mansfield and Grannell independently published work showing "one dimensional images," i.e., projections of a human finger with encoding along a single axis at 13 μm spatial resolution[2].

From these efforts an entire industry has emerged — magnetic resonance imaging (MRI). At present there are more than 3500 systems in the US alone. Virtually all of these efforts

have been directed at clinical imaging devices with spatial resolution generally ~ 10 mm^3. MR microscopy (MRM), on the other hand, has produced images with spatial resolution on the order of 1000 cubic micrometers, thus incurring a 10 million-fold reduction in signal intensity per volume element. The MR microscope predicted by the earliest researchers is only now becoming a reality as high temperature superconductors (HTS) are being utilized to remove one of the crucial barriers to spatial resolution; a low signal-to-noise ratio (SNR)[3]. As the MR microscope is commercialized, its impact in materials science, environmental science, biological science, and medicine will no doubt be comparable to that of clinical magnetic resonance imaging[4]. The key to this commercialization is the refinement of suitable high-temperature superconducting detectors.

II. Resolution Limits in MR imaging:

Each pixel in an MR image represents the signal from an encoded volume (voxel) of tissue. Typical clinical systems selectively excite slices of 3–10 mm with spatial encoding in the plane of the selected slices at ~ 1 x 1 mm. We define resolution then in terms of the three dimensional volume elements, e.g., 1 x 1 x 10 mm, or 10 mm^3.

The resolution limits in MRM are defined at some level by technology and at some level by fundamental physical laws[5,6,7,8,9]. The fundamental resolution limit in MRM will eventually be imposed by some combination of effects arising from spin lattice relaxation, diffusion, and/or magnetic susceptibility variations, all of which vary greatly from sample-to-sample. To date, there has been relatively little experimental verification of theoretical limits imposed by these effects since the technology has only recently evolved to the point where such experiments are possible.

The first technological barrier is imposed by the magnetic field gradients used for spatial encoding. For Fourier encoding, the gradient, G, and bandwidth of the receiver, $\Delta\omega$, can be related via the Larmor equation to the resolution, Δx, along the frequency encoding direction as follows:

$$\omega=\gamma B_0 ;$$
$$\Delta\omega=\gamma\Delta B.$$

But

$$\Delta B=GN\Delta x,$$

which leads to

$$\Delta x=\Delta\omega/\gamma GN,$$

where γ is the gyromagnetic ratio and N is the number of discrete points sampled with resolution Δx. Over the last several years there has been significant progress in the development of gradients, leading to commercial gradient coils that produce linear field

gradients of up to 100 Gauss/cm[10]. Typical clinical systems have gradients of ~ 1 Gauss/cm. Stronger gradients will most probably be necessary. Ahn et al.[11], and more recently McFarland[12], have predicted gradient strengths required for a given set of conditions based upon diffusion losses and kinetic arguments.

To date, however, the limited SNR in an MRM experiment has been the principal technical barrier to achieving resolution at the fundamental limits. The practical problems of increasing the SNR have been the subject of numerous publications[13,14,15]. One can scale the radio frequency (rf) coils to couple more tightly to a smaller specimen, improve the efficiency of the encoding sequences, and manipulate the relaxation recovery (T_1) and decay (T_2) times to achieve improvements. Operating at a higher magnetic field strength also improves SNR. Still, it turns out that the noise of the receiving coil itself becomes the limiting factor in achieving the best possible performance in MRM.

Recently a significant breakthrough was achieved in the battle for improved SNR through the development of the first high temperature superconducting rf detector for use with high-field MR imaging[3]. For larger samples, e.g., patients, the sample constitutes the main source of the noise. However for smaller samples, the rf detector can become the dominant noise source. Under these conditions, which are the conditions encountered in MR microscopy, reducing the noise from the coil through the use of a cooled superconducting rf detector can yield major improvements. An improvement of a factor of 30 over an equivalent copper coil was obtained in this first work. We note that imaging time goes *inversely as the square* of SNR. HTS technology is the breakthrough necessary to bring MRM to commercial fruition.

III. Contrast:

The single most significant element of MRI contributing to its clinical success is not the spatial resolution but the contrast resolution. The spatial resolution of a typical (x-ray) computed tomographic scan at 0.4 x 0.4 x 1 mm resolution is more than 5–10 X higher resolution than the highest resolution MRI image. The strength of MRI comes from its superb ability to delineate small differences in soft tissues. For example, the contrast difference in the grey and white matter of the brain on a CT scan is due to differences in x-ray absorption and is generally less than 0.5%. The contrast difference between grey and white matter in a "T_1 weighted" MR image can be > 20%. Moreover, many (if not most) pathologies, e.g., edema, inflammation, necrosis, and tumors, exhibit significant changes in parameters detected in MR images.

Thus the strength of MRI is that it detects changes in tissue parameters that are sensitive to pathology. The first clinical applications of MRI used differences in tissue spin-lattice relaxation time (T_1), and spin-spin relaxation time (T_2) to delineate and characterize pathologies[16]. As MRI has matured, a range of other molecular parameters have been found to be useful. For example, ischemic tissue, i.e., tissue damaged by stroke, is evident immediately in MR images which have been acquired with diffusion weighting, i.e., with a weighting dependent on local tissue viscosity, and the Brownian motion of water through the tissues[17 18]. Recently, great excitement has been generated in using sequences

in which the contrast is derived from local (microscopic) variation in magnetic fields. So called "functional images" demonstrating regions of local brain activity are thought to originate from local changes in flow and changes in blood as hemoglobin shifts from a diamagnetic state (oxy-hemoglobin) to a paramagnetic state (deoxy-hemoglobin) in regions of increased activity[19]. On many commercial systems there may be as many as fifty different imaging schemes to differentiate tissues based on parameters including T_1, T_2, proton density, diffusion, chemical shift information, perfusion, flow, etc.

Contrast in MR microscopy is related to, but significantly different from, that of its clinical cousin, MRI. Operation at higher magnetic fields in MRM (> 7 T vs. 1.5 T for clinical MRI) causes significant change in tissue T_1 and T_2 which are both field dependent[20,21]. Any contrast mechanism that is linked to susceptibility differences is very field dependent, since magnetic susceptibility effects scale as B^2. In addition, the use of very strong gradients in MRM, typically 100 X greater than those of the clinical systems, imposes many changes in contrast driven by diffusion coefficient differences in the tissues. Finally, interactions between these several effects, e.g., diffusion and susceptibility, are very poorly understood. Thus the large body of information on contrast in different tissues and pathologies available for clinical MRI is not available for the MR microscopist. A key element of this program has been to understand the contrast mechanisms involved in MR microscopy.

IV. Discussion:

The key to commercialization of MR histology is reduction of the total scan time. All of the essential technologies for this time reduction have been demonstrated in some form at the Center for In Vivo Microscopy (CIVM) in the Duke University Medical Center. The HTS probe demonstrated by Black and colleagues, coupled to recently developed high speed imaging pulse sequences developed in the CIVM will allow imaging at < 20 μm resolution in-plane, with acquisition times of 10–15 minutes[22] . Integrating all of the technologies —probe, sampling strategies, sample preparation, and MR pulse sequences, will be a nontrivial engineering effort but there are no fundamental physical barriers.

The key knowledge base that must be developed for the commercialization of MR histology is an understanding of the physical basis of the contrast mechanisms and clinical application of this knowledge to determine which mechanisms will most clearly define which pathology. It is most easily related to conventional pathology by examining the most routine stain —hematoxylin and eosin (H&E). Hematoxylin stains nucleic acids blue while eosin stains protein pink. A pathologist can determine that cells are "rapidly proliferating" in an H&E stained specimen by discerning an increase in blue nuclei over the pink background of protein in the cytosol. Size and uniformity of cell and different cell type become an additional clue. An example of a mechanism that will be relevant in MRM is the effect of cell size on T_2. Since there is a subtle but significant diamagnetic susceptibility difference between cells and the extracellular space, there are microscopic magnetic field gradients at the cell boundaries. Since these gradients are present over the voxel dimensions that obtain in MRM (5–15 μm), diffusion of protons through the gradients will alter local T_2.

The project described here was focused to develop the technology and knowledge base to answer the question "at what field should the MR microscope operate for effective MR histology?" Our previous work has clearly demonstrated that the technology can be applied. The work is not speculative. The HTS materials are very close to mass manufacture so there will be few barriers to commercialization. Commercialization of the MR microscope will take place even in the era of reduced medical funding because the cost savings from improved diagnosis with the device will easily justify the modest cost of the instrument. MR microscopy using HTS detectors will be widely available in less than five years.

Other Programs

At least two other groups have carried out technology development similar to ours, more or less simultaneously. J. Wosik of the University of Houston studied the use of HTS as an alternative to implanted coils for imaging of the spinal cord of small animals.[23] He employed a liquid nitrogen cryostat in which the coils were immersed. The animal was placed on top of the cryostat. A large, room temperature copper loop placed closer to the animal was used for transmission and for coupling inductively to the HTS coil. The coils were patterned YBCO films on 2" $LaAlO_3$ substrates. The measurements were done in the 2 T small animal MRI scanner operated by Ponnada Narayana at the University of Texas Health Science Center at Houston. Calculations were used to predict a gain of about 2 over a room temperature copper coil of the same size and distance from the animal, at 84 MHz. The animal was modeled as a cylinder of length 60 mm with a conductivity of 1 S/m. The point of interest was taken to be 5 mm deep. The coil was rectangular, 15 by 30 mm. Body to coil distance was assumed to be 10 mm.

J. R. Miller at Columbia University has used an HTS receiver coil to improve sensitivity for ^{23}Na imaging.[24] The coil was 24 mm in diameter and consisted of $Tl_2Ba_2CaCu_2O_8$ on a $LaAlO_3$ substrate. A separate transmitter coil was used. In the 3 T polarizing field, ^{23}Na has a resonance of 33.8 MHz. Inductive coupling to a cold pickup coil was used. Images of a phantom containing 30 mM Na solution showed a significant increase in SNR. The phantom was found to load the coil Q down from 20,000 to 2500. The coil was operated at a temperature of 40 K. The distance to the room temperature sample as held to only 4 mm.

HTS Coil Development

Cooling Apparatus

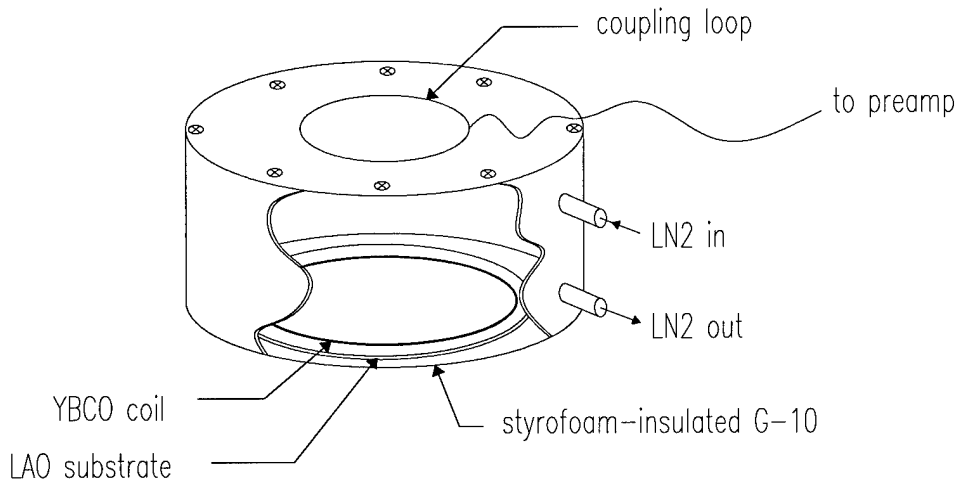

Figure 1. Cooling assembly for HTS coil.

In order to cool the coils in the magnet, a simple can with a removable top was constructed from standard G-10 fiberglass as shown in Figure 1. A thin layer of closed-cell styrofoam was affixed to outside of the can by means of epoxy. The coil was placed into the bottom of the can where it was held in place by a Delrin tray. Later, the Delrin was found to have excessive RF loss and was replaced the CIVM by a simple foam block. The can was meant to be cooled by a stream of liquid nitrogen. In practice, better results were sometimes achieved by shutting off the nitrogen flow during the imaging time. A flat cover was held down by eight screws to seal the assembly. Inductive matching was possible with a large loop at the back of the assembly. The thin layer of stryofoam was not intended to be sufficient to keep the outside of the housing at room temperature. Rather, the can was meant to be used in conjunction with a corrugated blanket through which warm air is forced. The coil and can are placed on one side of the blanket, the sample on the other.

Coil Designs

In order to accomplish the objectives of the research plan, coils were needed to allow ^{1}H and ^{3}He imaging at 2.0 T. The coils were designed according to several criteria. They were made as large as possible within the constraints of a 2" wafer to allow both small animal and specimen imaging. The coils do not require any capacitor or other external component to resonate at the Larmor frequency. They require only a single-sided film, which not only reduces cost but allows the comparison of films from deposition systems that are not designed to produce double-sided films. The coils are patterned from film on substrates of $LaAl0_3$, which consistently exhibit a Tc that is higher than films on sapphire.

Finally, the coils are also designed to minimize loss in the sample by minimizing the stray electric field.

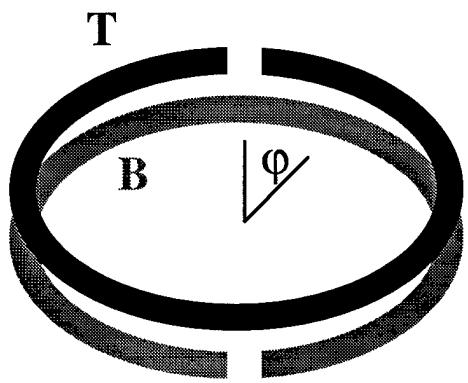

Figure 2. Split-ring coil.

In order to simultaneously fulfill the design criteria, the chosen approach was to make a single-sided version of the split-C resonator used successfully in the 9.4 T HTS microscopy probe developed by Black.[3] The split-ring uses the parallel-plate capacitance developed between the opposite sides of a double sided film to balance the inductance of a loop. The basic design is illustrated by Figure 2, with the substrate omitted for clarity. T indicates the top layer, and B the bottom. The desired resonant mode of the structure can be understood by applying simple differential equations and boundary conditions. By applying the conservation of current, $I_T(\varphi) + I_B(\varphi) = I$, we can derive the governing differential equations:

$$dV_T/d\varphi = dV_B/d\varphi = j\omega LI$$
$$dI_T/d\varphi = -dI_B/d\varphi = -j\omega C(V_T - V_B),$$

where L and C are the inductance and capacitance per unit angle. The relevant boundary conditions for the split ring coil are:

$$I_T(0) = 0 \quad I_B(\pi) = 0$$
$$I = \pi\omega C(V_T - V_B)$$
$$V_T - V_B = \pi\omega LI.$$

Combining the above yields:

$$\omega = 1/\pi(LC)^{1/2}$$

Converting to total inductance $\mathcal{L}$ and capacitance $\mathcal{C}$:

$$\mathcal{L} = 2\pi L, \ \mathcal{C} = 2\pi C$$
$$\omega = 1/(\mathcal{L}\mathcal{C}/4)^{1/2}$$

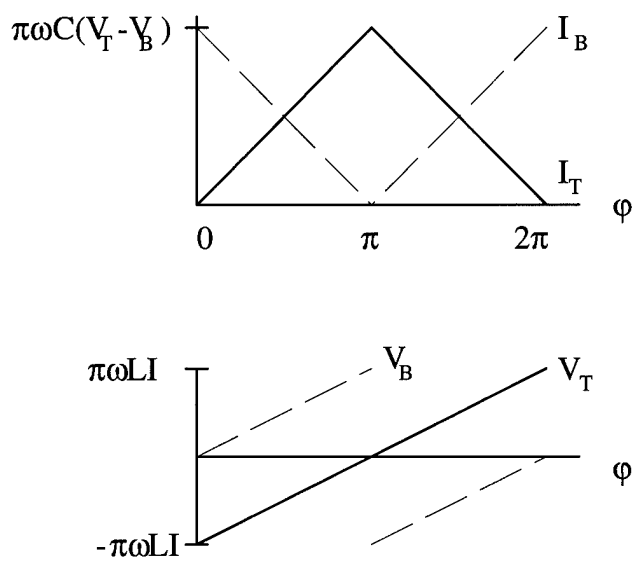

Figure 3. Voltage and current in split-ring coil.

The voltage and current as a function of angle are given in Figure 3. Another useful coil design, the two-turn spiral, shown in Figure 4, allows for a lower resonance frequency but produces a larger stray electric field, as we shall see from a similar analysis. Here we

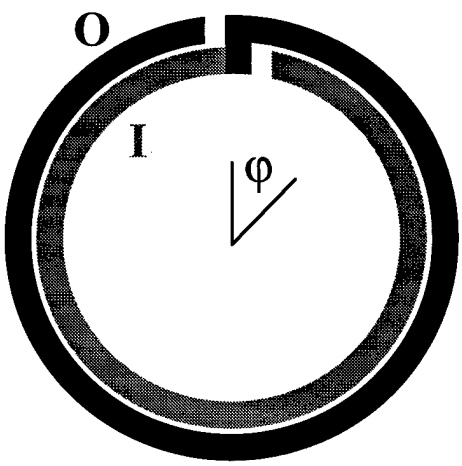

Figure 4. Two-turn spiral.

label the turns I and O, for inner and outer, but the expression for current conservation and the differential equations are the same:

$I_O(\varphi) + I_I(\varphi) = I$
$dV_O/d\varphi = dV_I/d\varphi = j\omega LI$
$dI_O/d\varphi = -dI_I/d\varphi = -j\omega C(V_O - V_I)$

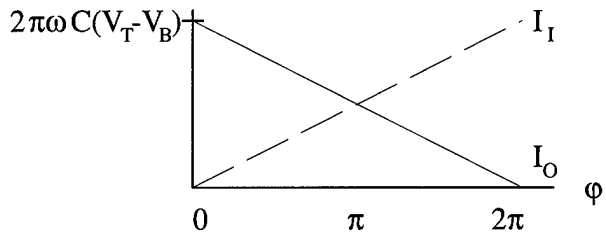

The boundary conditions are different:

$I_I(0_+) = 0 \quad I_O(2\pi_-) = 0$

The resulting solutions are:

$I = 2\pi\omega C(V_O - V_I)$
$V_O - V_I = 2\pi\omega LI$

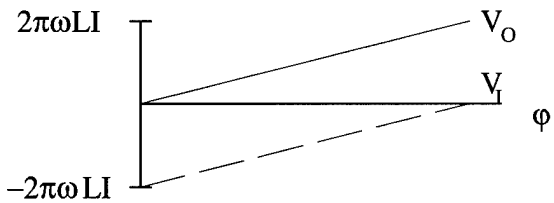

Figure 5. Voltage and current of two-turn spiral.

combining the above yields a resonance frequency:

$\omega = 1/2\pi(LC)^{\wedge}1/2$

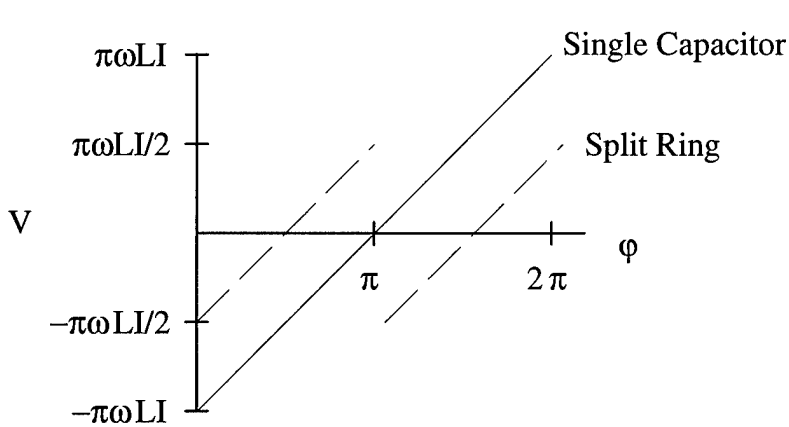

Figure 6. Comparison of average voltage around split-ring and two-turn spiral coils.

Converting to total inductance $\mathcal{L}$ and capacitance $\mathcal{C}$,

$\mathcal{L} = 2\pi L$, $\mathcal{C} = 2\pi C$
$\omega = 1/(\mathcal{L}\mathcal{C})^{\wedge}1/2$.

Note that the resonance of the two-turn spiral is lower for the same capacitance density.

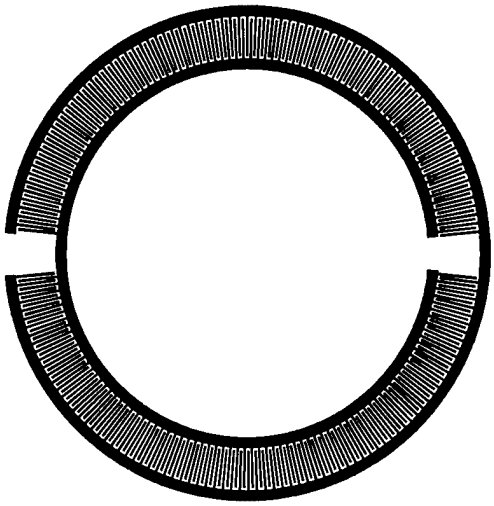

Figure 7. MRM6 is an example of a split-ring coil.

The electric field present in the sample is determined by the distribution of voltage around the coil. If the coil turns are much closer to each other than to the sample, it is possible to derive the electric field from the average of the voltage of the inner and outer (or top and bottom) turns. Figure 6 shows that the average voltage of the split-ring coil is one-half for the same total current. The resulting electric field at the sample will be consequently be lower. Both electric-field loss and detuning will be reduced by the split-ring design. To construct a split-ring coil with a single-sided film, it is necessary to nest one ring inside the other. To a first approximation we can neglect the difference in diameter. The capacitance is developed between the edges of the rings. In practice it is often useful to lower the resonance frequency by introducing fingers between the inner and outer rings to increase the capacitance. The capacitor formed is a common type of microstrip component known as an interdigital capacitor. Unlike the parallel plate capacitor in the original split-ring design, the interdigital capacitor is sensitive to the dielectric parameters of its environment. For example, because the dielectric constant of liquid nitrogen is 1.4 while for liquid helium it is only 1.04, the resonance frequency will be lower in liquid nitrogen. Figure 7 showns an implementation of a such single-sided split ring design that is designated MRM6. When constructed on $LaAlO_3$ it resonates at about 84 Mhz, as required for ^1H NMR at 2.0 T. MRM6 has 318 fingers, each of which is 206 μm wide. The gap between the fingers is 207 μm. The outer diameter is 47 mm, the inner diameter is 35 mm. Table 1 is a list of the coil designs developed in conjunction with this contract. All coils had inner and outer diameters of 35 and 47 mm, respectively. The RF behavior of the coils was simulated with IE3D (Zeeland Software), an integral-equation electromagnetic solver, to help determine the frequency of resonance.

Device Name	Number of fingers	Finger Width (μm)	Finger Gap (μm)	Resonance (MHz)
MRM1	526	126	250	77.7
MRM2	306	216	250	99.7
MRM5	310	212	211	86.7
MRM6	318	206	207	85.0
MRM7	330	200	189	81.7
MRM8	753	88	87	58.2

Table 1. Coil designs.

Coil Fabrication and Testing

Films were deposited, patterned, and tested at Conductus. Tuning was carried out by means of laser trimming, if needed. Coils were passivated with teflon and shipped to the CIVM, where they were retested for resonance frequency and Q-factor in and out of the

magnetic field. Coils which were of an appropriate frequency and maintained a reasonable Q in field were used for magnetic resonance.

Table 2 lists the coils that were manufactured for the project in order of the date patterned. Coils patterned before the actual term of the contract have been included below, although the work was not charged to the contract. The film number is a Conductus designation that allows films to be tracked easily. As shown in Table 3, the prefix of the film number indicates the source of the film. All films were deposited at Conductus except for ones with a prefix of G, which were purchased from Technical University of Munich at Garching. Niobium films are numbered only by date of deposition, and are used primarily to check tuning.

Date patterned	Film Number	Mater-ial	Design	Film Thickness (μm)	Freq. (MHz)
1/12/95	011094	Nb	MRM 4	1.0	99.2
1/12/95	011194	Nb	MRM1	1.0	77.7
1/1295	011294	Nb	MRM2	1.0	99.7
2/28/95	3-101894A	YBCO	MRM1	0.60	76.4
3/22/95	032295	Nb	MRM5		86.7
3/22/95	032295	Nb	MRM8		58.2
3/24/95	3-032395A	YBCO	MRM6	0.36	84.8
4/16/95	3-040695B	YBCO	MRM6	0.36	83.9
4/25/95	595-036	YBCO	MRM6	0.40	85.5
5/3/95	595-065	YBCO	MRM6	0.40	85.9
5/6/95	595-067	YBCO	MRM8	0.40	58.7
10/18/95	G-090895-2	YBCO	MRM6	0.30	85.1
10/18/95	G-090895-1	YBCO	MRM6		85.7
11/15/95	895044C	YBCO	MRM8		
11/15/95	895043A	YBCO	MRM6		84.9
11/15/95	895044E	YBCO	MRM8	0.40	
3/20/96	G-090895-10	YBCO	MRM7	0.30	81.7
5/1/96	G-090895-11	YBCO	MRM6	0.30	84.7
5/1/96	G-090895-12	YBCO	MRM6	0.30	85.0

Table 2. Process report for coils.

Film number	Deposition system
595-nnn	off-axis laser ablation
895nnn	high-throughput sputtering
3-date	small sputtering chamber
G-date-serial number	Garching

Table 3. Key to sources of YBCO film.

As of January 30 1996 a total of 5 HTS coils had been delivered to the CIVM: 4 resonated at 85 MHz for 2 T proton imaging, 1 resonated at 65 MHz for 2 T helium imaging (see Table 4). The coils were designed, modeled, fabricated, tested and tuned at Conductus before being sent to the CIVM. There, the coils are retested for resonance frequency and Q-factor inside and outside the 2 T magnet. At Conductus, the coils were tested in a dipping probe that held the coil between two plates of G-10 fiberglass. Then the coils were retested at the CIVM, both in the G-10 housing described above and in a simple foam bucket filled with liquid nitrogen. The G-10 housing was operated in a flow mode. The coil was

supported by a Delrin structure. To cool the 2" coil, liquid nitrogen was forced under pressure to flow through the G-10 dewar. Inside the housing, the coil surface was flush with the liquid nitrogen level. Coupling was achieved by means of an external, room-temperature loop. The position of the loop was varied until a power match to a 50 Ω transmission line was achieved. Tuning was not adjusted in the magnet. Instead, the shift in frequency between the bench and magnet was noted and incorporated into the bench-tuning procedure.

There were a number of difficulties encountered with this setup. Principally, the frequency stability and reproducibility of the coils (crucial since no tuning in the magnet was provided) were poor. The flowing liquid nitrogen was believed to cause actual motion of the coil. Certainly, turbulence and bubbles of gas in the liquid nitrogen stream contributed to frequency instability. The Delrin support structure proved to have excessive RF loss, and was replaced with a block of open-cell foam. The experiment time was limited to a period of about 40 minutes before the sample, a phantom, froze.

Some of these coils were damaged in handling. Mylar tape was applied to the film of MRM6/595-036 in an attempt to improve the stability of the resonance frequency, damaging some of the fingers. MRM6/595-065 was exposed to moisture when unpassivated, and consequently had a very poor Q.

It was not clear how much of the deQing in the magnet was due to the field and how much was due to interaction with structures in the magnet wall--specifically, the gradient and shim coils. The coil was normally placed off-center in the magnet, adding to the possibility of inductive coupling to the gradient coils. To test this hypothesis a warm copper shield was placed between MRM6/G-090895-1 and the magnet wall. The coil was resting in a styrofoam bucket filled with liquid nitrogen. With the shield in position the in-field Q increased by 50 % from 2600 to 3900. Since the coil had a Q of 9,700 out of field in liquid nitrogen, evidently significant deQing occurred both due to the field and to coupling to the gradients.

There is some indication that the temperature of the coils in the G-10 housing is not 77 K.

		Q @ -14 dBm				
		Out of field			In field	
Design	Film number	LHe G-10 dipping probe	LN_2 G-10 housing	LN_2 styrofoam housing	LN_2 G-10 housing	LN_2 styrofoam housing
MRM6	595-036	8,800	1,200	N/A	800	N/A
MRM6	595-065	6,600	2,500	N/A	1000	N/A
MRM6	895043A	4,100	2,500	5,100	250	490
MRM6	G-090895-1	11,300	9,700	11,300	950	2,600
MRM8	595-067	9,300	7,000	6,000	3000	N/A

Table 4. Q factors of coils delivered to CIVM before January 30, 1996.

	Q (-14 dBm)
in LHe	11800
in LN_2	11000
in LN_2 at CIVM	9000
in LN_2 at field	1700
as above, w. shield	3000

Table 5. Measured Q's of MRM6/G-090895-2.

MRM6/895043A exhibited significantly higher Q in the foam dewar both in and out of the field. The film also deQed by about an order of magnitude when placed in the 2 T field. This is at least consistent with the interpretation that the film had a depressed critical temperature, and so was sensitive to small variations in temperature above 77 K. MRM6/G-090895-1 also exhibited a higher Q in the foam dewar than in the G-10 housing.

The most promising of the coils listed in Table 4, MRM6/G-090895-1 and MRM8/595-067, resonated slightly too high in frequency. They were returned to Conductus on February 9 to be tuned down slightly. The coils were vacuum-sealed into food-service style bags against disks of 30 mil teflon sheet. The teflon pressed directly against the film comprising the interdigital capacitors. Since teflon has a higher dielectric constant (2) than liquid nitrogen (1.4), the frequency of the coil was slightly reduced. The resonance frequency of MRM6/G-090895-1 was reduced from 86.1 to 85.7 MHz on the bench. Unfortunately, MRM8/595-067 shattered when it was sealed against the teflon disk. It appeared that the stress of flattening the teflon sheet was enough to break the fragile $LaAlO_3$ substrate. A significant benefit of the teflon disk is that by keeping the liquid nitrogen away from the interdigital capacitors, the packaging significantly improved both the Q and a the stability of the resonance. With a teflon washer, the measured Q of MRM6/G-090895-1 improved from 11,300 to 13,400. Wear on coils due to handling is also reduced. With the higher measured Q, we were able to observe loading effects from steel supports in our lab bench and rebar in the floor, and took steps to avoid them. One addtional coil, MRM6/G-090895-2, was delivered to CIVM sealed with a teflon disk. Its measured Q's are given in Table 5. Unlike the values in Table 4, these measurements were made with the teflon disk in place.

Initial images at the CIVM were obtained with a gravity-driven system to reduce turbulence and avoid leakage of liquid nitrogen. Results were unsatisfactory due to poor control of flow rate. In late February, the use of a pressured supply dewar was initiated. Better sealing of the cryostat allowed some pressurization without leakage. Improved coil stabilization reduced vibration and the resultant frequency instability and improved SNR.

Some significant problems with stability remained at the beginning of April. Images still had some excess phase encode noise, and coils were difficult to tune and match in place. Stability was greatly improved by shutting off the flow to a cold probe and imaging in the several minutes that the probe remained cold. A variety of configurations to tune and match the coils have been tested.

Tuning is accomplished with sheets of copper at room temperature which can be moved to vary the degree of inductive loading placed on the coil. The coil is not significantly deQed by the sheets, so there is probably little degradation in noise temperature

associated with tuning. Some tests of resonant loops have also been made, but have not yet shown significant advantages over the copper sheets.

Matching to the coils is done inductively, and loops have been tested both in and outside the cryostat. The cryostat design, while it keeps size to a minimum, requires any coax penetrating the shell to drop in temperature by more that 200 K over less than 2 cm of length. We experienced problems with coaxial lines freezing in place and causing the liquid nitrogen to boil, reducing stability. Greater success was achieved by allowing the matching loop to remain at room temperature outside the cryostat.

Surface coil imaging with HTS coils

Images of a 28 mm diameter tube of magnevist-doped H_20 obtained with both HTS and room-temperature copper coils are shown in Figure 8. Visible in the images are dark spots which are due to a set of plastic rods arrayed approximately parallel to the axis of the tube. The phantom loaded the coils only lightly. A 2D spin-echo sequence was used, with TR/TE = 300/10 ms, and bandwidth of 62.5 KHz. One average was collected in a scan time of 38 seconds. The field of view was 5 x 5 cm, the slice thickness 3 mm. A 256 x 128 data set was collected and zero-filled to 256 x 256. The distance between the coil and sample is the same for the copper and HTS coils: about 5 mm.

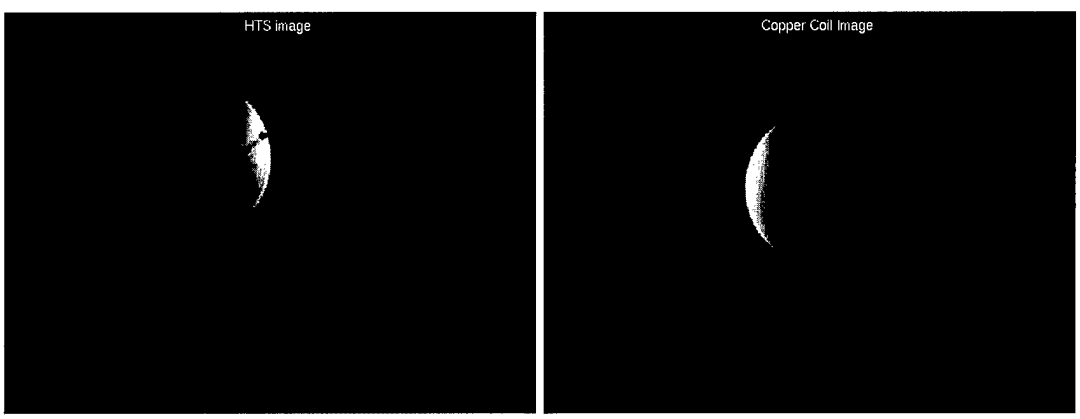

Figure 8. Images of a H_20 phantom with HTS and copper coils.

The HTS image of Figure 8 was obtained with MRM6/ G-090895-1. When tuned and placed in the magnet in the G-10 housing the coil was measured to have a Q of about 950. The coil was cooled by liquid nitrogen flowing through the cryostat continuously. The copper coil was of a double-sided split-ring design, fabricated on a microwave substrate to have the same inner and outer dimensions (and resonance frequency) as the HTS design. The copper coil had a Q of about 160. A MATLAB script was used to produce SNR plots for each image, which are reproduced in Figure 9. Plots through the center of each image are displayed in Figure 10, and show that the SNR in the HTS image is 1.9 times higher than in the copper coil. Note that the apparent offset in the SNR curves is present only for clarity. The offset does not indicate the absence of a vacuum wall for the copper coil. Somewhat better results with the copper coil could be achieved by moving it closer to the sample.

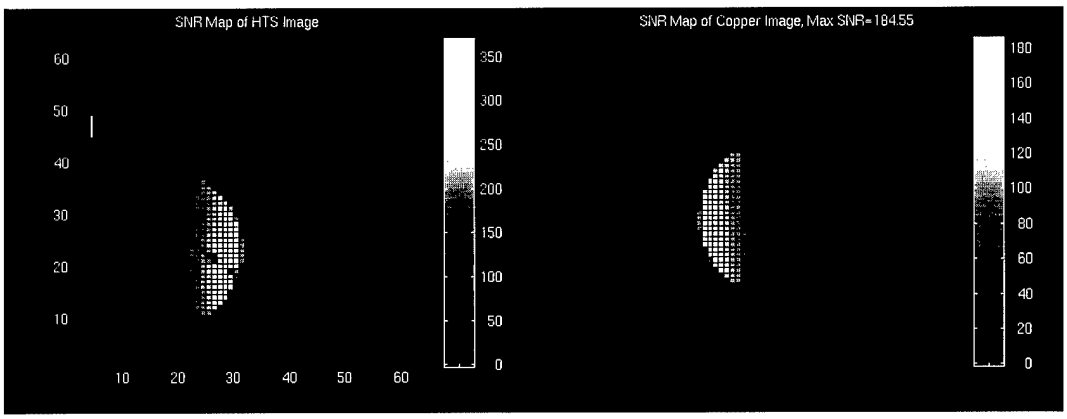

Figure 9. SNR maps of images from HTS and copper coils.

Taking the SNR as proportional to $\sqrt{Q/T}$ (neglecting sample loading and preamp temperature), and assuming that the noise temperature of the coil is 77 K, the predicted SNR gain is x4.8, more than twice what we achieved.

If, however, the coil Q is dominated by loss from structures at 300 K (cryostat, gradient coils) then the noise temperature of the HTS coil is nearly 300 K, and we would have predicted SNR gain of 2.4 due to Q alone. This is in reasonable agreement with the data, and will be investigated by direct measurement of the noise temperature.

The HTS image above has a much higher level of phase encode noise than the copper image, which may also explain part of the non-ideal SNR gain. This is illustrated by the images in Figure 11, which are windowed to display noise.

Dramatic reduction in phase-encode noise in the HTS image was obtained by shutting off the liquid nitrogen flow during the imaging sequence, as shown in Figure 12. The coil would stay cold for several minutes after flow was terminated. Subsequently, the addition of a baffle allowed stable imaging even with liquid nitrogen flow.

The HTS coil was shown to provide a factor of 2 improvement in SNR for nonloading samples even with a Q of 900 and probably a high noise temperature. Cryogenics and inductive tuning and matching worked well enough to image a phantom.

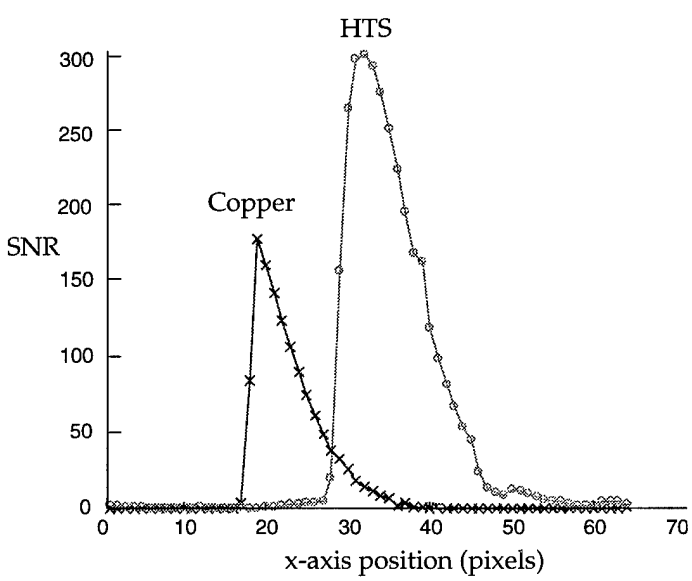

Figure 10. SNR of HTS and copper coils.

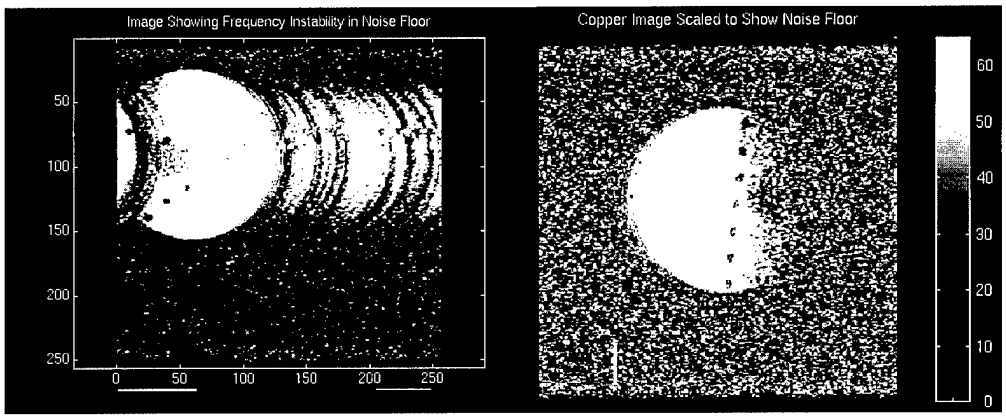

Figure 11. Relative phase noise with HTS and copper coils.

Although images demonstrating significant SNR gains over copper coils were obtained in the third quarter of the contract, significant questions remained regarding the level of SNR gain achieved, and the suitability of liquid nitrogen as a cryogen. Milestones for the final quarter were selected to address these questions on a basic level. These milestones included measuring the extent of coil deQing in the magnet, accounting for the observed SNR gain, and testing a liquid nitrogen reservoir to replace the flow system.

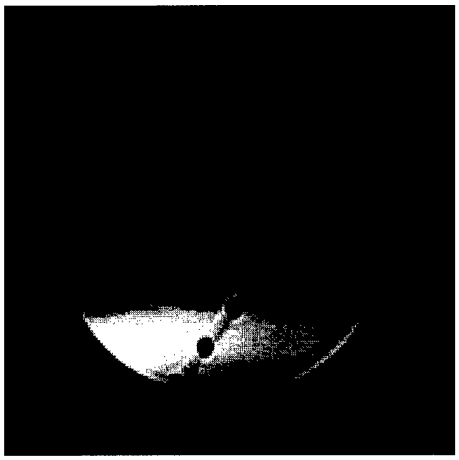

Figure 12. HTS image of 28 mm diameter phantom acquired with nitrogen flow cut off.

In order to obtain images of biological samples, the only new obstacle to be overcome was the need to keep the coil holder from causing the biological sample to freeze. On July 8 and 9, a corrugated sheet with air flowing through it to keep the sample warm was tested. The sample remained at room temperature while the coil cooled normally. It should now be possible to obtain images of biological samples as desired.

Two more coils were fabricated and sent to Duke at the beginning of June. Table 6 gives the results of bench tests at Conductus in liquid nitrogen with teflon disks sealed to the coils as described above.

Noise tests were conducted by setting up the scanner as normal, but without a sample. Coil MRM6/G-090895-11 was used. At field, the Q dropped to 1700. The image in Figure 13 was acquired. The readout, or frequency axis, is vertical. The distribution of noise intensity with respect to the vertical axis indicates the quality of noise match to the

Design	Film number	Resonance freq. (Mhz)	Q (-15 dBm, 0 T)
MRM6	G-090895-11	84.7	17,500
MRM6	G-090895-12	85.0	8,600

Table 6. Performance of final coils sent to Duke.

coil. The presence of a clear horizontal stripe demonstrates the narrow bandwidth of the coil in which it is matched to the preamp. The noise temperature of the coil is given by the noise level at the center of the stripe, the frequency at which the coil is matched to the preamp. Images were also acquired with the coil replaced by a resistor--first at room temperature and then in liquid nitrogen. The level of the noise band was comparable to the level of the hot resistor, indicating that the effective temperature of the coil is approximately 300 K. We infer that the coil is picking up noise (and probably substantial deQing) from some external source--probably the gradient coil. It is also possible that the noise comes from dielectric loading from some warm material in the coil holder. Taking into account the measured noise temperature of the HTS coil leads to a predicted SNR gain of 2.4 due to Q alone. This is in reasonable agreement with the measured SNR. To investigate the source of the deQing one might use smaller coils that would interact less with the environment and give a truer measure of field-induced deQing.

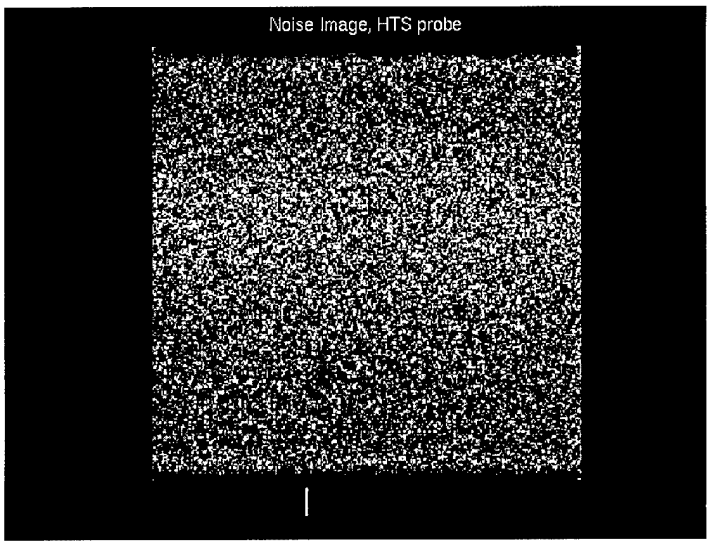

Figure 13. Noise image of HTS coil.

Significant deQing of the coils in the magnet has been consistently observed. If the observed coil deQing is due to the magnetic field, it may be appropriate to shift our attention to approaches to cooling the coils that will reduce the operating temperature. A mixed gas system would cool the coils to about 60 K, compared to the 77 K achieved with liquid nitrogen. To examine the effect of the magnetic field on the coil resonance, the Q and frequency vs. field (in units of position) of coil MRM6/G-090895-12 were measured. Q dropped as the coil was inserted into the bore. It was hypothesized that the coil temperature might be above 77 K, and substituted another coil holder. It is a model #1155 Thermos, and is used as a nitrogen reservoir rather than a flow system. With the new cooler, the Q further improved. Also, changing the coil orientation in field changed the Q. In the styrofoam dewar it dropped from 3200 to 620 when turned perpendicular to the field. Out of field the same coil had a Q of 10,000.

There was some concern that the effects of the magnetic field were confused with the effects of loading due to external structures. To reduce coupling between the coil and any external structures, we tested a smaller coil, an MRM3B/895044H that had been patterned on lanthanum aluminate. A sheet of teflon was placed sealed against the coil in a vacuum bag to reduce loading from liquid nitrogen. Bench tests at Conductus showed a Q in liquid nitrogen with 0 dBm to the coil of 10,000. At Duke, a Q of 5,500 out of the magnet with about -15 dBm to the coil was measured. It is not known why the Q at Duke

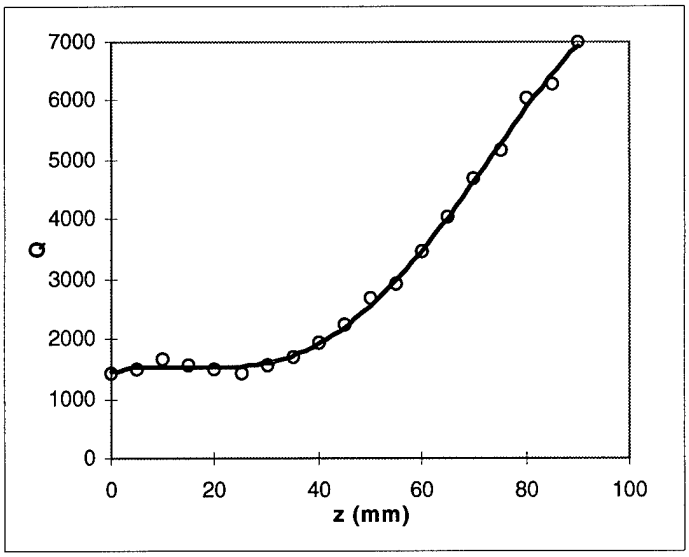

Figure 14. Q as function of axial position. z=0 is the center of the magnet.

was so much lower. In a 2 T field with a shield, the Q dropped to 700. We know that there is significant film-to-film variation in the effect of a magnetic field. This may just be a particularly sensitive film.

The Field Dependence of Contrast to Noise in Magnetic Resonance Microscopy

The traditional approach to increasing the signal to noise ratio (SNR) has been to increase the polarization by operation at higher magnetic fields. But as one moves to higher field, the spin-lattice and spin-spin relaxation times, T_1 and T_2, also change[25,26]. T_1 and T_2 determine the contrast in an image. In addition, for specific imaging strategies (pulse sequences) , changes in T_1 and T_2 can produce significant changes in SNR. Thus both the contrast and signal to noise will change with magnetic field.

The specific goal of this research is a systematic simulation of the change in contrast to noise (CNR) as a function of magnetic field. Our hypothesis is that the substantial increase in SNR achieved with HTS coils, combined with specific imaging strategies, and reasonable assumptions about the constrast mechanisms may lead one to an intermediate magnetic field where the CNR might be optimal.

Field Dependence of Signal to Noise

The field dependence of SNR is given by equation 1 below:

$$SNR \propto \frac{\omega^2}{\sqrt{a\omega^2 \quad + b\omega^{1/2}}} \qquad [1]$$

where ω is the Larmor frequency, and a and b are constants that are dependent on the conductivity and geometry of the sample and coil, respectively. Depending on the relative magnitude of the coil and sample noise, expressed in the denominator above, we consider two extremes SNR $\propto \omega^{7/4}$ or SNR $\propto \omega$.

Field Dependence of T_1

The contrast in any given situation is dependent on the tissues involved, their T_1, and the field dependence of the respective T_1's. The analytic dependence of T_1 has been studied by a number of authors who generally use some sort of polynomial fit. We generalize our study by modeling the T_1 with a Fermi function shown in equation 2.

$$T1 = a_1 + a_2 \left\{ a_3 - \frac{1}{1 + \frac{1}{a_5} e^{\left(B_0 - a_4\right)}} \right\} \qquad [2]$$

The dependence matches qualitatively the experimental results of Koenig et. al[27]. The model executed in MATLAB accepts a five element array (a_{1-5}) that characterizes completely the T1 curve of a particular type of tissue. Examples are shown in Figure 15.

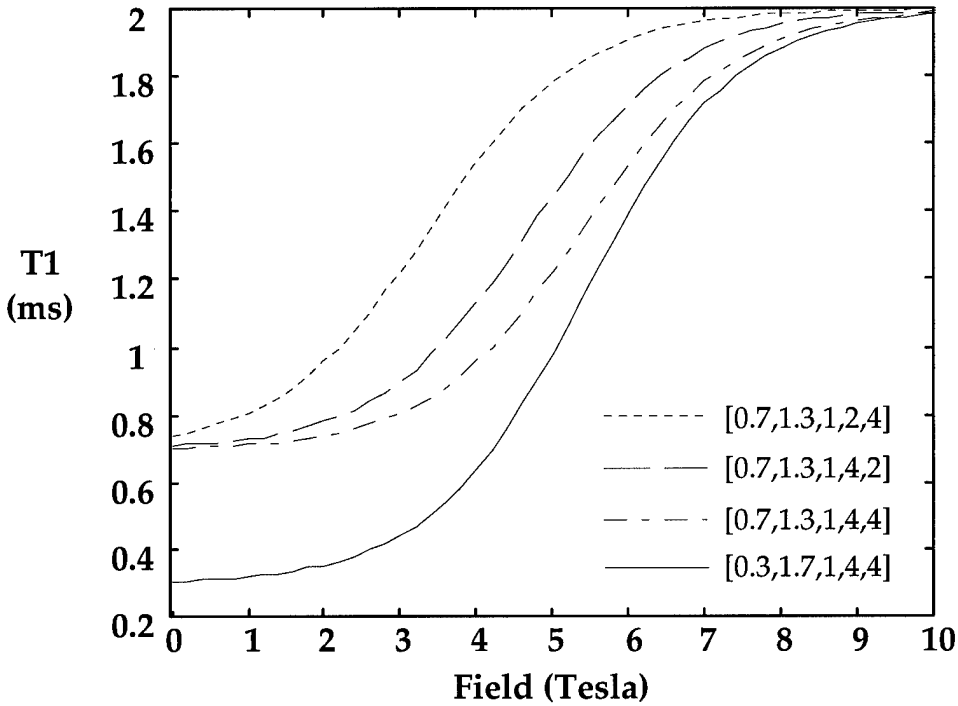

Figure 15. T_1 vs field modeled using a Fermi function for 4 types of tissue described by selected input arrays (a1-5).

We have selected a typical example of T_1 dependence. Nota Bene: we do not suggest that the model for T_1 dependence below is quantitative, only qualitative. Specifically we believe that the field dependence of T_1 levels off at a much lower magnetic field than that we use in our model. Our interest at this point is to determine if in fact there might be an "optimum" field, i.e. a maximum in the contrast to noise that occurs at something other than the highest field . By choosing the range (to 10 T) we conservatively weight our estimate in favor of maximizing CNR at the highest possible field. If a lower "optimum " exists, we can be reasonably confident in the model. The absolute value of that optimum would, after all, be determined by the specific field dependence of the T1's of the tissues, parameters that will vary from tissue to tissue.

Contrast to Noise

The field dependence of contrast to noise will depend on the pulse sequence as well as the contrast mechanism. Our first order model uses a fixed bandwidth, partial saturation sequence with a fixed echo (TE=5 ms) and repetition time (TR=400 ms)

We assume a signal dependence for T1 of tissues a and b (each having its own set of "a" parameters) as in equation 3.

$$S_{a,b} = (1 - e^{-TR / T_{1a,b}}) \qquad [3]$$

The contrast C is given by

$$C = \frac{S_a - S_b}{S_a + S_b} \qquad [4]$$

The contrast to noise ratio (CNR) will depend specifically on how the noise scales with frequency. We assume that the SNR will scale as ω^n where n ranges from 1 to 7/4. With these assumptions, the model yields the CNR shown in Figure 16.

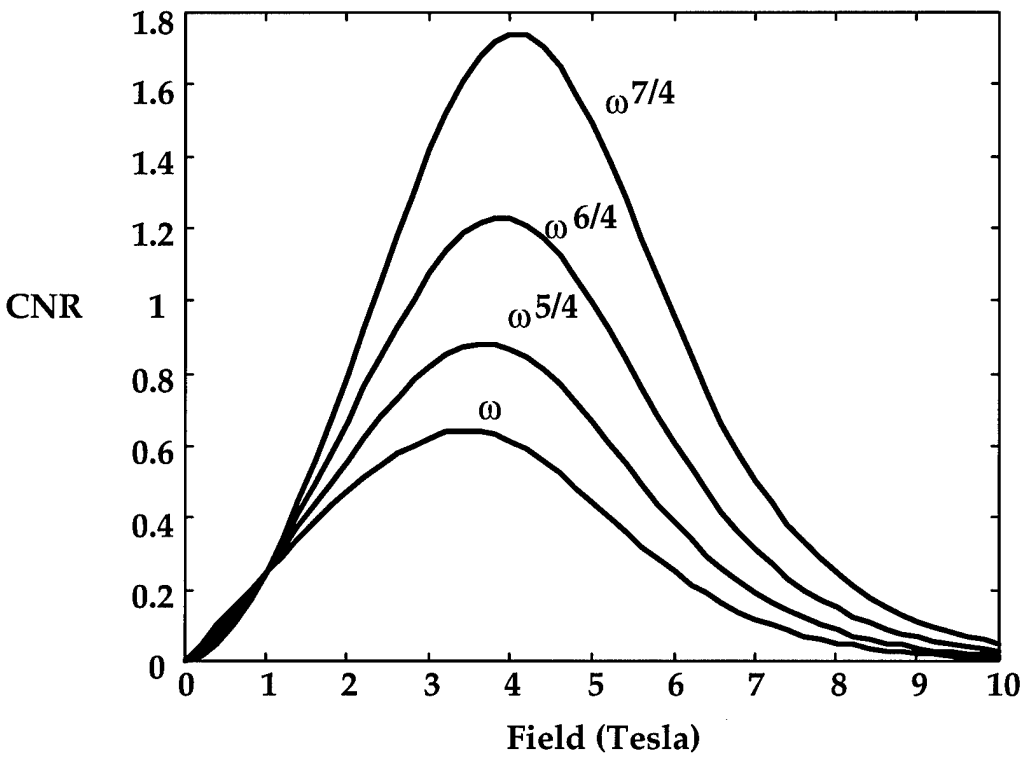

Figure 16. Field dependence of the contrast to noise ratio for a T1 weighted imaging sequence.

Conclusion

Figure 16 strongly supports the initial hypothesis that there may in fact be a magnetic field at which the contrast to noise is an optimum. The exact field is dependent primarily on the field dependence of T_1. We have made very conservative estimates so that we do not unfairly favor our hypothesis. The optimum field between 3 and 5 T arises because our T_1 model (Figure 2) shows the most rapid changes in this field range. Careful review of Koenig's data suggests that this probably occurs at a much lower field[28,29,30]. This

argues strongly for the development of an MR microscope with an HTS detector at fields ranging between 0.5 and 1.0 T.

Conclusions

Technology Development

A feasibility study for a magnetic resonance microscope has been performed. Sensitivity is the key technical issue to developing a practical NMR microscope for clinical applications. Two issues that are crucial to sensitivity have been evaluated: the strength of the polarizing field and the design of the RF coil. The results point to a new strategy for providing high contrast and resolution in a relatively inexpensive, compact instrument.

The optimal strength of the polarizing field was evaluated based on published studies of the relaxation parameters of biological tissue. The measure of image quality was taken to be the contrast to noise ratio (CNR) of a T_1 weighted image. For a wide range of relaxation parameters there was a pronounced peak in the CNR between 1 and 2 T. The choice of such a magnetic field would dramatically reduce the cost and size of the final instrument.

The performance of HTS and copper RF coils was compared in a 2.0 T MRI system, and the HTS coils were found to give superior sensitivity. Even under conditions that were far from ideal, a factor of two improvement in sensitivity was obtained with HTS coils cooled by liquid nitrogen. The 77 K temperature provided by liquid nitrogen was found to be cold enough to provide significant sensitivity improvement. However, the coil performance at the 2.0 T field was compromised compared to performance on the bench. A colder, preferably closed-cycle, refrigeration system would significantly improve the performance of the HTS coil beyond what was demonstrated.

Potential Applications

The applications of MRM cover a range of disciplines. As electron microscopy, confocal microscopy, phase contrast microscopy, even conventional light microscopy span a wide range of fields, so too will MRM find uses in a broad range of applications. The majority of applications to date have focused on biological systems, most probably due to the origins of most of the MRI research and access to systems. A number of investigators have ventured into new areas, including studies of porous media, studies in elastomers, chemical diffusion, and ceramics, to name but a few. While the principal focus of this program is on biological applications, applications in porous media and plant sciences give a hint of the breadth of applications in MRM.

One can define two broad categories for application of MRM in the biological sciences: in vivo and in vitro studies. The majority of biomedical applications of MRM have been in vivo studies, again most probably arising from the logical extension of clinical applications to animal models of disease.

There is, for example, great interest by the pharmaceutical industry in using MRM in vivo to follow the time course of disease and response to therapies [4]. Present techniques employing conventional histology are extremely expensive. A typical study used to evaluate the potential of a new pharmaceutical might employ 50 control animals and 50 treated animals sacrificed at each of three to five points in the time course of a therapeutic intervention —a total of 500 small animals. Large numbers of animals are necessary at each evaluation point to obtain appropriate statistics to account for biological diversity and variability in response. Upon sacrifice, the appropriate tissues are sectioned and stained for conventional histology with subsequent evaluation by a trained pathologist — an exceptionally costly step. Consider 50–100 sections for each animal, which must be carefully surveyed by a highly trained pathologist, and the complexity and expense of the process becomes apparent. MR microscopy has the potential to significantly reduce cost and complexity, significantly reduce the number of animals required, and to provide statistically much more sound data. Since MRM is nondestructive, each animal can frequently act as its own control. The details are dependent on the disease model, but typically an animal can be studied before a disease process is initiated, e.g., surgical creation of a stroke. The same animal can then be studied at multiple time points in the evolution of the disease and/or with a pharmaceutical agent under study. One can see a region of the brain affected by stroke and watch that region **in the same animal** as the agent under study is administered. Studies with as few as 20 animals become very meaningful, with reduction in costs of as much as 10–100 X.

Bibliography

Hurlston, S., Black, R.D., Brey, W.W., Chen, X.J., Hedlund, L.W., Withers, R.S., Yap, M., Johnson, G.A. A superconducting surface coil for in vivo MR microscopy. Book of Abstracts, Fourth Scientific Meeting, International Society for Magnetic Resonance in Medicine. New York, April 27 - May 3, 1996.

References

[1] Lauterbur PC. Image formation by induced local interactions - examples employing nuclear magnetic resonance. Nature 1973; 242: 190-191.

[2] Mansfield P and Grannell PK. Diffraction in microscopy in solids and liquids by NMR. Phys. Rev. B 1975; 12: 3618.

[3] Black RD, Early TA, Roemer PB, et al. A high temperature superconducting receiver for NMR microscopy. Science 1993; 259: 793-795.

[4] Johnson GA, Benveniste H, Black RD, et al. MR Microscopy of Disease Models. In: Blumich B and Kuhn W, eds., Magnetic Resonance Microscopy: Methods and Applications in Materials Science and Biomedicine. Weinheim, Germany: VCH Publishers, 1992:501-511.

[5]Callaghan PT and Eccles CD. Sensitivity and resolution in NMR imaging. J. Magn. Reson. 1987; 71: 426-445.

[6] Callaghan PT and Eccles CD. Diffusion-limited resolution in nuclear magnetic resonance microscopy. J. Magn. Reson. 1988; 78: 1-8.

[7] Callaghan PT. Susceptibility-limited resolution in nuclear magnetic resonance microscopy. J. Magn. Reson. 1990; 87: 304-318.

[8] Cho ZH, Ahn CB, Juh SC, et al. NMR Microscopy with 4 μm resolution - theoretical study and experimental results. Med. Phys. 1988; 15: 815-823.

[9] Hyslop WB and Lauterbur PC. Effects of restricted diffusion on microscopic NMR imaging. J. Magn. Reson. 1991; 94: 501-510.

[10] Roemer PB, Edelstein WA, and Hickey JS. Self shielded gradient coils. In: Proc. Soc. Magn. Reson. Med. Montreal, Canada, 1986:1067.

[11] Ahn CB and Cho ZH. A generalized formulation of diffusion effects in μm resolution nuclear magnetic resonance imaging. Med. Phys. 1989; 16(1): 22-28.

[12] McFarland E. Time independent point-spread function for MR microscopy. Magn. Reson. Imaging 1992; 10: 269-278.

[13] Hoult DI and Richards RE. The signal to noise ratio of the nuclear magnetic resonance experiment. J. Magn. Reson. 1976; 24: 71-85.

[14] Karis JP, Johnson GA, and Glover GH. Signal to noise improvements in three dimensional NMR microscopy using limited angle excitation. J. Magn. Reson. 1987; 71: 24-33.

[15] Maki JH, Johnson GA, Cofer GP, and MacFall JR. SNR improvement in NMR microscopy using DEFT. J. Magn. Reson. 1988; 80: 482-492.

[16] Herfkens R, Davis P, Crooks L, et al. NMR imaging of the abnormal live rat and correlations with tissue characteristics. Radiology 1981; 141: 211-219.

[17] Moseley ME, Cohen Y, and Montorovitch J et al. Early detection of regional cerebral ischemia in cats; comparison of diffusion and T2 weighted MRI and spectroscopy. J. Magn. Reson. 1990; 14: 330-345.

[18] Benveniste H, Hedlund LW, and Johnson GA. Mechanism of detection of acute cerebral ischemia in rats by diffusion-weighted magnetic resonance microscopy. Stroke 1992; 23: 746-754.

[19] Belliveau JW, Kennedy DN, McKinstry RC, et al. Functional mapping of the human visual cortex by magnetic resonance imaging. Science 1991; 254: 716-719.

[20] Johnson GA, Herfkens RJ, and Brown MA. Tissue relaxation time: *in vivo* field dependence. Radiology 1985; 156: 805-810.

[21] Dockery SE, Suddarth SA, and Johnson GA. Relaxation measurements at 300 MHz using MR microscopy. Magn. Reson. Med. 1989; 11(2): 182-192.

[22] Zhou X, Cofer GP, Suddarth SA, and Johnson GA. High Field MR microscopy using fast spin echoes. Magn. Reson. Med. 1993; 30: 60–67.

[23] Wosik J, Nesteruk K, Xie LM, Zhang XP, Gierlowski P, Jiao C, Miller JH, Enhanced-Resolution Magnetic Resonance Imaging Using High-Tc Superconducting rf Receiver Coils, Proceedings of the 10th Anniversary HTS Workshop on Physics, Materials and Applications, Houston, Texas, March 12-16, 1996.

[24]Miller JR, Zhang K, Ma QY, Mun IK, Jung KJ, Katz J, Face DW, Kountz DJ, High Temperature Superconducting Receiver Coils for Sodium Imaging, Book of Abstracts, Fourth Scientific Meeting, International Society for Magnetic Resonance in Medicine. New York, April 27 - May 3, 1996.

[25]Johnson GA, Herfkens RJ, Brown MA, Tissue relaxation time: *in vivo* field dependence. Radiology 1985; 156: 805-810.

[26]Dockery SE, Suddarth SA, Johnson GA, Relaxation measurements at 300 MHz using MR microscopy. Magn. Reson. Med. 1989; 11: 182-192.

[27]Koenig SH, Brown RD, Adams D, Emerson D, Harrison CG, Magnetic field dependence of $1/T_1$ protons in tissue. Invest. Radiol. 1984; 19: 76-81.

[28]Koenig SH, Baglin C, Brown RD, Brewer CR, Magnetic field dependence of solvent proton relaxation induced by Gd3+ and Mn2+ complexes. Magn. Reson. Med. 1984; 1: 496-501.

[29]Gillis P, Koenig SH, Transverse relaxation of solvent protons induced by magnetized spheres: application to ferritin, erythrocytes, and magnetite. Magn. Reson. Med. 1987; 5: 323-345.

[30]Koenig SH, A theory of solvent relaxation by solute clusters of noninteracting paramagnetic ions, as exemplified by ferritin. Magn. Reson. Med. 1985; 2: 873-874.